Available online at www.sciencedirect.com
ScienceDirect
Solid State Communications 143 (2007) 110–115
solid state communications
www.elsevier.com/locate/ssc

Electrons in bilayer graphene

Edward McCann, David S.L. Abergel*, Vladimir I. Fal'ko

Department of Physics, Lancaster University, Lancaster, LA1 4YB, UK

Accepted 2 March 2007 by A. Geim
Available online 27 April 2007

Abstract

Electrons in bilayer graphene possess an unusual property: they are chiral quasiparticles characterized by Berry phase 2π. We review the tight-binding model of bilayer graphene which determines the band structure and low-energy quasiparticle properties of this material and we describe the optical manifestation of the existence of a pair of split-bands and low-energy branches in the bilayer spectrum. Then, we analyze the stability of a bilayer with respect to a ferroelectric transition and we model the self-consistent control of the interlayer asymmetry gap induced by a transverse electric field in a graphene-based field-effect transistor.

PACS: 81.05.Tp; 71.20.-b; 73.23.-b; 78.30.-j

Keywords: A. Nanostructures; D. Electronic band structure; D. Optical properties; D. Electronic transport

1. Introduction

Following the fabrication of monolayer graphene [1], the observation of an unusual sequencing of quantum Hall effect plateaus [2] was explained in terms of Dirac-like chiral quasiparticles with Berry phase π [3–6]. Subsequently, bilayer graphene became a subject of intense interest in its own right. This followed the realization that the low energy Hamiltonian of a bilayer describes chiral quasiparticles with a parabolic dispersion and Berry phase 2π [7] as confirmed by quantum Hall effect [8] and ARPES measurements [9].

The electronic band structure of bilayer graphene has been modelled using both density functional theory [10–12] and the tight-binding model [13,7,14–17]. It has been predicted [7] that asymmetry between the on-site energies in the layers leads to a tunable gap between the conduction and valence bands. The dependence of the gap on external gate voltage has been modelled taking into account screening within the tight binding model [16,17,12] and such calculations appear to be in good agreement with ARPES measurements [9], observations made in the regime of the quantum Hall effect [17], and density functional theory calculations [12].

The tight-binding model of bilayer graphene is reviewed in Section 2, including trigonal warping effects. Section 3 explains how the optical absorption coefficient of bilayer graphene is influenced by the presence and dispersion of pairs of electronic bands [18,19], in contrast to the featureless absorption coefficient of monolayer graphene. We obtain the effective low energy Hamiltonian of bilayer graphene in Section 4 and we show that it is dominated by chiral quasiparticles with a parabolic dispersion and Berry phase 2π. Section 5 describes the opening of a gap in bilayer graphene due to layer asymmetry with a demonstration that an undoped, gapless bilayer is stable with respect to the opening of a gap, followed by a calculation using a self-consistent Hartree approximation to describe the control of the gap in the presence of an external gate.

2. The tight-binding model of bilayer graphene

We consider bilayer graphene to consist of two coupled hexagonal lattices with inequivalent sites $A1$, $B1$ and $A2$, $B2$ on the bottom and top graphene sheets, respectively, arranged according to Bernal ($A2$–$B1$) stacking: as shown in Fig. 1(a), every $B1$ site in the bottom layer lies directly below an $A2$ site in the upper layer, but sites $A1$ and $B2$ do not lie directly below or above a site in the other layer. We

* Corresponding author.
E-mail address: daveabergel@googlemail.com (D.S.L. Abergel).

0038-1098/$ - see front matter © 2007 Elsevier Ltd. All rights reserved.
doi:10.1016/j.ssc.2007.03.054

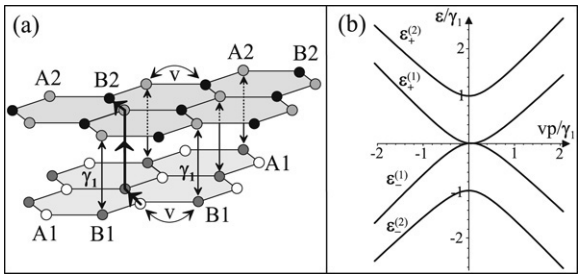

Fig. 1. (a) Schematic of the bilayer lattice containing four sites in the unit cell: $A1$ (white circles) and $B1$ (grey) in the bottom layer, and $A2$ (grey) and $B2$ (black) in the top layer. (b) Schematic of the low energy bands near the K point obtained by taking into account intralayer hopping with velocity v, $B1A2$ interlayer coupling γ_1, $A1B2$ interlayer coupling γ_3 [with $v_3/v = 0.1$] and zero layer asymmetry Δ.

employ the tight-binding model of graphite [20] by adapting the Slonczewski–Weiss–McClure parameterization [21,22] of relevant couplings in order to model bilayer graphene. In-plane hopping is parameterized by coupling $\gamma_{A1B1} = \gamma_{A2B2} \equiv \gamma_0$ and it leads to the in-plane velocity $v = (\sqrt{3}/2)a\gamma_0/\hbar$ where a is the lattice constant. In addition, we take into account the strongest inter-layer coupling, $\gamma_{A2B1} \equiv \gamma_1$, between pairs of $A2$–$B1$ orbitals that lie directly below and above each other. Such strong coupling produces dimers from these pairs of $A2$–$B1$ orbitals, leading to the formation of high energy bands [7]. We also include weaker $A1$–$B2$ coupling $\gamma_{A1B2} \equiv \gamma_3$ that leads to an effective velocity $v_3 = (\sqrt{3}/2)a\gamma_3/\hbar$ where $v_3 \ll v$. Here, we write the Hamiltonian [7] near the centres of the valleys in a basis corresponding to wave functions $\Psi = (\psi_{A1}, \psi_{B2}, \psi_{A2}, \psi_{B1})$ in the valley K [23] and of $\Psi = (\psi_{B2}, \psi_{A1}, \psi_{B1}, \psi_{A2})$ in the valley $\tilde{K}$:

$$\mathcal{H} = \xi \begin{pmatrix} -\frac{1}{2}\Delta & v_3\pi & 0 & v\pi^\dagger \\ v_3\pi^\dagger & \frac{1}{2}\Delta & v\pi & 0 \\ 0 & v\pi^\dagger & \frac{1}{2}\Delta & \xi\gamma_1 \\ v\pi & 0 & \xi\gamma_1 & -\frac{1}{2}\Delta \end{pmatrix}, \tag{1}$$

where $\pi = p_x + \mathrm{i}p_y$, $\pi^\dagger = p_x - \mathrm{i}p_y$, $\mathbf{p} = (p_x, p_y) \equiv p(\cos\phi, \sin\phi)$ is the momentum measured with respect to the K point, $\xi = +1(-1)$ labels valley K ($\tilde{K}$). The Hamiltonian takes into account asymmetry $\Delta = \epsilon_2 - \epsilon_1$ between on-site energies in the two layers, $\epsilon_2 = \frac{1}{2}\Delta$, $\epsilon_1 = -\frac{1}{2}\Delta$.

At zero magnetic field, the Hamiltonian $\mathcal{H}$ has four valley-degenerate bands [7], $\epsilon_\pm^{(\alpha)}(\mathbf{p})$, $\alpha = 1, 2$, with

$$\epsilon_\pm^{(\alpha)2} = \frac{\gamma_1^2}{2} + \frac{\Delta^2}{4} + \left(v^2 + \frac{v_3^2}{2}\right)p^2 + (-1)^\alpha\sqrt{\Gamma}$$

$$\Gamma = \frac{1}{4}\left(\gamma_1^2 - v_3^2p^2\right)^2 + v^2p^2\left[\gamma_1^2 + \Delta^2 + v_3^2p^2\right] + 2\xi\gamma_1v_3v^2p^3\cos 3\phi. \tag{2}$$

They are plotted in Fig. 1(b) for $\Delta = 0$ and $v_3/v = 0.1$. The dispersion $\epsilon_\pm^{(2)}$ describes two bands with energies $\epsilon_+^{(2)} \geq \gamma_1$ and $\epsilon_-^{(2)} \leq \gamma_1$: they do not touch at the K point. These bands are the result of strong interlayer coupling $\gamma_{A2B1} \equiv \gamma_1$ which forms 'dimers' from pairs of $A2$–$B1$ orbitals that lie directly below and above each other [7].

The dispersion $\epsilon_\pm^{(1)}(p)$ describes low energy bands that touch at the K point in the absence of layer asymmetry $\Delta = 0$. In the intermediate energy range, $\frac{1}{4}\gamma_1(v_3/v)^2$, $|\Delta| < |\epsilon_1| < \gamma_1$, it can be approximated [7] with

$$\epsilon_\pm^{(1)} \approx \pm\frac{1}{2}\gamma_1\left[\sqrt{1 + 4v^2p^2/\gamma_1^2} - 1\right]. \tag{3}$$

This interpolates between a linear spectrum $|\epsilon_\pm^{(1)}| \approx vp$ at high momenta and a quadratic spectrum $|\epsilon_\pm^{(1)}| \approx p^2/2m$, where $m = \gamma_1/2v^2$. Such a crossover happens at $p \approx \gamma_1/2v$, which corresponds to the carrier density $n^* \approx \gamma_1^2/(4\pi\hbar^2v^2)$. This is lower than the density at which the higher energy band $\epsilon^{(2)}$ becomes occupied $n^{(2)} \approx 2\gamma_1^2/(\pi\hbar^2v^2) \approx 8n^*$. Using experimental graphite values [22] gives $n^* \approx 4.36 \times 10^{12}$ cm^{-2} and $n^{(2)} \approx 3.49 \times 10^{13}$ cm^{-2}. The estimated effective mass m is light: $m = \gamma_1/2v^2 \approx 0.054m_e$.

3. Optical absorption of bilayer graphene

The electromagnetic field absorption in graphene has been studied in a number of publications [24,18,19,25,26]. We show that the bilayer absorption coefficient can be described as

$$g_2 = (2\pi e^2/\hbar c)\, f_2(\omega), \tag{4}$$

and it is qualitatively different from the featureless monolayer absorption coefficient $g_1 = \pi e^2/\hbar c$, since g_2 reflects the presence and dispersion of two pairs of bands in bilayer graphene [18,19] as described in Section 2 and Fig. 1(b).

We characterize the polarization of the EM field $\mathbf{E}_\omega = \boldsymbol{\ell}Ee^{-\mathrm{i}\omega t}$ by denoting the vector $\boldsymbol{\ell}_\oplus = (\mathbf{l}_x - \mathrm{i}\mathbf{l}_y)/\sqrt{2}$ to correspond to right-hand circular polarization and the vector $\boldsymbol{\ell}_\ominus = (\mathbf{l}_x + \mathrm{i}\mathbf{l}_y)/\sqrt{2}$ to be the left-handed circularly polarized light. In a 2D electron gas with conductivity $\sigma(\omega) \ll c/2\pi$, absorption of an EM field arriving along the direction antiparallel to a magnetic field can be characterized by the ratio of the Joule heating and the energy flux $\mathbf{S} = c\mathbf{E}\times\mathbf{H}/4\pi = -S\mathbf{l}_z$ transported by the EM field so that $g \equiv E_iE_j^*\sigma_{ij}(\omega)/S$. Using the Keldysh technique, we express

$$g = \frac{8e^2}{c\omega}\Re\int\frac{F\mathrm{d}\epsilon}{N}\widehat{\mathrm{Tr}}\left\{\hat{v}_i\ell_i\hat{G}^R(\epsilon)\hat{v}_j\ell_j^*\hat{G}^A(\epsilon+\omega)\right\},$$

where $\hat{\mathbf{v}} = \partial_{\mathbf{p}}\mathcal{H}$ is the velocity operator, $\widehat{\mathrm{Tr}}$ includes the summation both over the sublattice indices "tr" and over single-particle orbital states, N is the normalization area of the sample and $F = n_\mathrm{F}(\epsilon) - n_\mathrm{F}(\epsilon+\omega)$ takes into account the occupancy of the initial and final states and includes spin and valley degeneracies.

We write the retarded and advanced Green's functions of electrons in the bilayer as $\hat{G}^{R/A}(\mathbf{p},\epsilon) = [\epsilon \pm \mathrm{i}\hbar/(2\tau) - \mathcal{H}(\mathbf{p})]^{-1}$ and the trace operation as $\widehat{\mathrm{Tr}} = \int\mathrm{d}^2\mathbf{p}\frac{N}{(2\pi\hbar)^2}\mathrm{tr}$. Neglecting the momentum transfer from light (since $\epsilon/c \sim 3 \times 10^{-3}$), reproduces [24,25] the constant absorption coefficient $g_1^\parallel =$

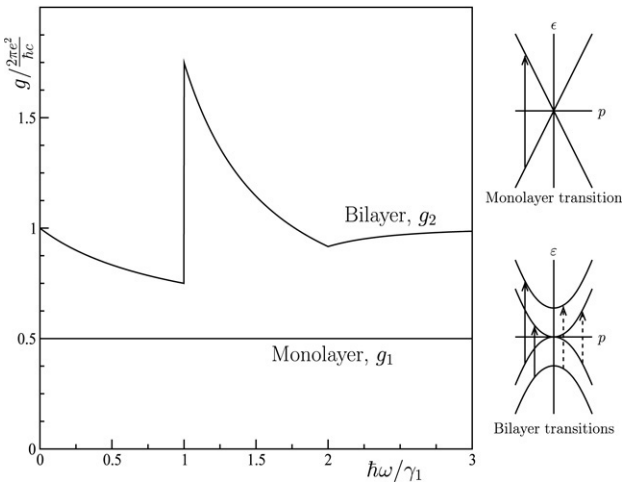

Fig. 2. Absorption coefficient of bilayer and monolayer graphene in the optical range of frequencies. The insets illustrate the quasiparticle dispersion branches in the vicinity of ϵ_F and possible optical transitions.

$\pi e^2\hbar c$ ($f_1 = \frac{1}{2}$) in monolayer graphene. Taking into account all four bands in the bilayer we arrive at the expression for the absorption coefficient for light polarized in the plane of the graphene sheet:

$$g_2^{\parallel} = \frac{2\pi e^2}{\hbar c} f_2(\Omega), \qquad \Omega \equiv \frac{\hbar\omega}{\gamma_1} > \frac{2|\epsilon_F|}{\gamma_1}, \tag{5}$$
$$f_2 = \frac{\Omega+2}{2(\Omega+1)} + \frac{\theta(\Omega-1)}{\Omega^2} + \frac{(\Omega-2)\theta(\Omega-2)}{2(\Omega-1)},$$

where $\theta(x<0)=0$ and $\theta(x>0)=1$ which agrees with the calculation by Nilsson et al. [18] in the clean limit and $T=0$. The frequency dependence [27] of the bilayer optical absorption is illustrated in Fig. 2 in comparison to that in a monolayer. It is the electron–hole excitation between the low energy band $\epsilon_{\pm}^{(1)}$ and the split band $\epsilon_{\pm}^{(2)}$ which provides the structure in the vicinity of $\hbar\omega = \gamma_1$ ($\gamma_1 \approx 0.4$ eV [22]). At high photon energies, $\hbar\omega \gg \gamma_1$, the frequency dependence saturates at $f=1$. The absorption coefficient for the left- and right-handed light are the same over the whole spectral interval, so Eq. (5) is also applicable to light linearly polarized in the graphene plane.

4. Effective low energy Hamiltonian

To describe the transport properties of bilayer graphene, it is convenient to use a low energy Hamiltonian that describes effective hopping between the non-dimer sites, $A1$–$B2$, i.e. those that do not lie directly below or above each other and are not strongly coupled by γ_1. This two component Hamiltonian was derived in [7] using Green's functions. Alternatively (and equivalently), one can view the eigenvalue equation of the four component Hamiltonian equation (1) as producing four simultaneous equations for components ψ_{A1}, ψ_{B2}, ψ_{A2}, ψ_{B1}. Eliminating the dimer state components ψ_{A2}, ψ_{B1} by substitution, and treating γ_1 as a large energy, gives the two component Hamiltonian [7] describing effective hopping between the $A1$–$B2$ sites:

$$\hat{H}_2 = -\frac{1}{2m}\begin{pmatrix} 0 & \left(\pi^{\dagger}\right)^2 \\ \pi^2 & 0 \end{pmatrix} + \hat{h}_w + \hat{h}_a; \tag{6}$$
$$\hat{h}_w = \xi v_3 \begin{pmatrix} 0 & \pi \\ \pi^{\dagger} & 0 \end{pmatrix}, \quad \text{where } \pi = p_x + \mathrm{i}p_y;$$
$$\hat{h}_a = -\xi\Delta\left[\frac{1}{2}\begin{pmatrix} 1 & 0 \\ 0 & -1 \end{pmatrix} - \frac{v^2}{\gamma_1^2}\begin{pmatrix} \pi^{\dagger}\pi & 0 \\ 0 & -\pi\pi^{\dagger} \end{pmatrix}\right].$$

The effective Hamiltonian $\hat{H}_2$ is applicable within the energy range $|\epsilon| < \frac{1}{4}\gamma_1$. In the valley K, $\xi = +1$, we determine $\Psi_{\xi=+1} = (\psi_{A1}, \psi_{B2})$, whereas in the valley $\tilde{K}$, $\xi = -1$, the order of components is reversed, $\Psi_{\xi=-1} = (\psi_{B2}, \psi_{A1})$. The Hamiltonian $\hat{H}_2$ describes two possible ways of $A1 \rightleftharpoons B2$ hopping. The first term takes into account $A1 \rightleftharpoons B2$ hopping via the $A2B1$ dimer state. Consider $A1$ to $B2$ hopping as illustrated with the thick solid line in Fig. 1(a). It includes three hops between sites: an intralayer hop from $A1$ to $B1$, followed by an interlayer transition via the dimer state $B1A2$, followed by an intralayer hop from $A2$ to $B2$. Since the two intralayer hops are both A to B, the first term in the Hamiltonian contains π^2 or $(\pi^{\dagger})^2$ on the off-diagonal with the mass $m = \gamma_1/2v^2$ reflecting the energetic cost γ_1 of a transition via the dimer state. This term in $\hat{H}_2$ yields a parabolic spectrum $\epsilon = \pm p^2/2m$ with $m = \gamma_1/2v^2$. It has been noticed [7] that quasiparticles described by it are chiral: their plane wave states are eigenstates of an operator $\boldsymbol{\sigma}\mathbf{n}_2$ with $\boldsymbol{\sigma}\mathbf{n}_2 = 1$ for electrons in the conduction band and $\boldsymbol{\sigma}\mathbf{n}_2 = -1$ for the valence band, where $\mathbf{n}_2(\mathbf{p}) = (\cos(2\phi), \sin(2\phi))$ for $\mathbf{p} = (p\cos\phi, p\sin\phi)$. Quasiparticles described by this term acquire a Berry phase 2π upon an adiabatic propagation along a closed orbit, thus charge carriers in a bilayer are Berry phase 2π quasiparticles, in contrast to Berry phase π particles in a monolayer [5].

The second term $\hat{h}_w$ in the Hamiltonian equation (6) describes weak direct $A1B2$ coupling, $\gamma_{A1B2} \equiv \gamma_3 \ll \gamma_1$. This coupling $\gamma_{A1B2} \equiv \gamma_3$ leads to the effective velocity $v_3 = (\sqrt{3}/2)a\gamma_3/\hbar$ where $v_3 \ll v$, Eq. (2). In a similar way to bulk graphite [21,28], the effect of coupling γ_3 is to produce trigonal warping, which deforms the isoenergetic lines along the directions $\phi = \phi_0$, as shown in Fig. 3(a). For the valley K, $\phi_0 = 0$, $\frac{2}{3}\pi$ and $\frac{4}{3}\pi$, whereas for $\tilde{K}$, $\phi_0 = \pi$, $\frac{1}{3}\pi$ and $\frac{5}{3}\pi$. The effective low energy Hamiltonian equation (6) yields the following energy for $\Delta = 0$,

$$\epsilon_{\pm}^{(1)2} \approx (v_3 p)^2 - \frac{\xi v_3 p^3}{m}\cos(3\phi) + \left(\frac{p^2}{2m}\right)^2, \tag{7}$$

which agrees with Eq. (2) in the low energy limit $|\epsilon| \ll \gamma_1$. At very low energies $|\epsilon| < \epsilon_L = \frac{1}{4}\gamma_1(v_3/v)^2 \approx 1$ meV, the effect of trigonal warping is dramatic. It leads to a Lifshitz transition: the isoenergetic line is broken into four pockets, which can be referred to as one "central" and three "leg" parts [28,7,29]. The central part and leg parts have minimum $|\epsilon| = \frac{1}{2}|\Delta|$ at $p = 0$ and at $|p| = \gamma_1 v_3/v^2$, angle ϕ_0, respectively. For $v_3 \ll v$, we find [7,22] that the separation of the 2D Fermi line into four pockets would take place for very small carrier

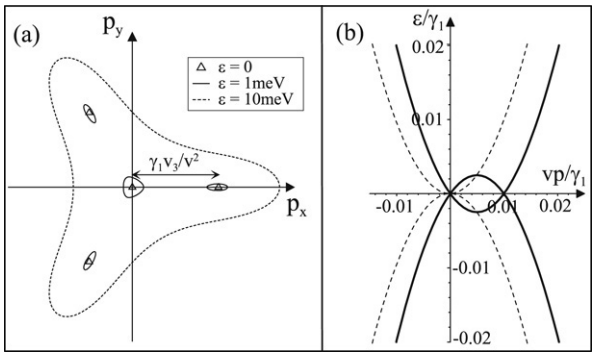

Fig. 3. (a) Schematic of the Fermi line at low energy in the valley K, $\xi = 1$, for different values of the Fermi energy. Note that the asymmetry of the Fermi line at the other valley, $\xi = -1$, is inverted. (b) The low energy bands plotted along the line $p_y = 0$. They are obtained by taking into account intralayer hopping with velocity v, $B1A2$ interlayer coupling γ_1, $A1B2$ interlayer coupling γ_3 [with $v_3/v = 0.1$] and zero layer asymmetry Δ. Dashed lines show the bands obtained by neglecting γ_3 [i.e. with $v_3/v = 0$].

densities $n < n_L \sim (v_3/v)^2 n^* \sim 1 \times 10^{11}\,\mathrm{cm}^{-2}$. In this estimation of n_L, the constant of proportionality is of the order 1 as determined by the strongly warped shape of the Fermi line at the Lifshitz transition. For $n < n_L$, the central part of the Fermi surface is approximately circular with area $\mathcal{A}_c \approx \pi\epsilon^2/(\hbar v_3)^2$, and each leg part is elliptical with area $\mathcal{A}_\ell \approx \frac{1}{3}\mathcal{A}_c$. The low energy part of the band structure is plotted in Fig. 3(b) along the line $p_y = 0$. Taking the line $p_y = 0$, $\phi = 0$, at the first valley $\xi = 1$ gives $\epsilon_\pm^{(1)} \approx \pm|v_3 p - p^2/(2m)|$. It shows that, at zero energy, the leg pocket of the Fermi surface develops at $p = 2mv_3 = \gamma_1 v_3/v^2$, Fig. 3(a), and that the overlap between the conduction and valence bands, Fig. 3(b), is given by $2\epsilon_L \approx (\gamma_1/2)(v_3/v)^2 \approx 2$ meV [15] using $\gamma_1 \approx 0.4$ eV and $v_3/v \approx 0.1$.

5. Stability of the bilayer against ferroelectric ordering and a voltage-controlled gap in the spectrum

The parameter Δ in the Hamiltonian equation (1) takes into account a possibly-externally-controlled asymmetry $\Delta = \epsilon_2 - \epsilon_1$ between on-site energies in the two layers, $\epsilon_2 = \frac{1}{2}\Delta$, $\epsilon_1 = -\frac{1}{2}\Delta$. The electronic bands near the K point, Eq. (2), are shown in Fig. 4(a) for a large value of the layer asymmetry Δ. For simplicity, we neglect $A1B2$ interlayer coupling γ_3:

$$\epsilon_\pm^{(\alpha)2} \approx \frac{\gamma_1^2}{2} + \frac{\Delta^2}{4} + v^2p^2 + (-1)^\alpha \sqrt{\frac{\gamma_1^4}{4} + v^2p^2\left(\gamma_1^2 + \Delta^2\right)}.$$

The energies of the bands exactly at the K point are $|\epsilon_\pm^{(2)}(p = 0)| = \sqrt{\gamma_1^2 + \Delta^2/4}$ and $|\epsilon_\pm^{(1)}(p = 0)| = |\Delta|/2$: the low energy bands, $\epsilon_\pm^{(1)}$, are split by the layer asymmetry Δ at the K point [30].

In an asymmetrical bilayer, the electronic densities on the individual layers, n_1 and n_2, are given by an integral with respect to momentum $p = \hbar|\mathbf{k}|$ over the circularly symmetric Fermi surface, taking into account the relative weight of the

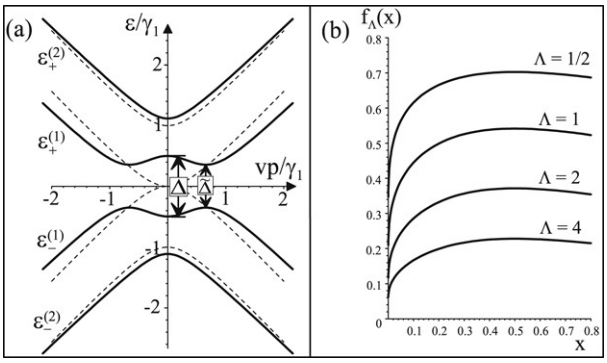

Fig. 4. (a) Schematic of the electronic bands near the K point in the presence of finite layer asymmetry Δ (for illustrative purposes a very large asymmetry $\Delta = \gamma_1$ is used) obtained by taking into account intralayer hopping with velocity v and $B1A2$ interlayer coupling γ_1, but neglecting $A1B2$ interlayer coupling γ_3. Dotted lines show the bands for zero asymmetry $\Delta = 0$. (b) Dependence of the function $f_\Lambda(x)$, Eq. (14), describing the density dependence of the layer asymmetry on the argument x for different values of the screening parameter Λ.

wave functions:

$$n_{1(2)} = \frac{2}{\pi\hbar^2}\int p\,\mathrm{d}p\left(|\psi_{A1(2)}(p)|^2 + |\psi_{B1(2)}(p)|^2\right), \qquad (8)$$

where we have included a factor of four to take into account spin and valley degeneracy. By determining the wavefunction amplitudes on the four separate atomic sites we find

$$n_{1(2)} = \int \mathrm{d}p\; p\, g_\mp(\epsilon, p), \qquad (9)$$

$$g_\mp(\epsilon, p) = \frac{\epsilon \mp \Delta/2}{\pi\hbar^2\epsilon}\left[\frac{\left(\epsilon^2 - \Delta^2/4\right)^2 \mp 2v^2p^2\epsilon\Delta - v^4p^4}{\left(\epsilon^2 - \Delta^2/4\right)^2 + v^2p^2\Delta^2 - v^4p^4}\right],$$

where the minus (plus) sign is for the first (second) layer.

We establish the stability of an undoped, gapless bilayer system with respect to ferroelectric ordering (redistribution of charge density between the two layers) by comparing the gain in the total energy due to the opening of a gap in the low energy spectrum with the energetic cost due to Coulomb energy E_c equal to that of a capacitor with oppositely charge plates. We estimate the charging energy by approximating the excess electronic densities on the individual layers, n_1 and n_2, as uniformly distributed within infinitesimally thin 2d layers. Then, the charging energy is $E_c = Q^2/2C_b$ where $Q = en_1L^2 = -en_2L^2$ is the excess charge on one of the layers in the presence of finite asymmetry $\Delta = \epsilon_2 - \epsilon_1$, and $C_b = \varepsilon_r\varepsilon_0L^2/c_0$ is the capacitance of a bilayer with interlayer separation c_0 and area L^2. For an undoped system, with Fermi energy $\epsilon_F = 0$ and zero excess total density $n_1 = -n_2$, we only need to consider the valence bands $\epsilon_-^{(1)}$ and $\epsilon_-^{(2)}$. On integrating Eq. (9) from zero momentum to a large momentum p_∞, and using an expansion in Δ/γ_1, we find that the change in the density of the valence bands for finite Δ, as compared to $\Delta = 0$, is

$$n_{1(2)} \approx \pm\frac{\gamma_1\Delta}{4\pi\hbar^2v^2}\ln\left(\frac{4\gamma_1}{|\Delta|}\right), \qquad (10)$$

and

$$E_c \approx \frac{e^2}{32\pi^2 C_b}\left(\frac{L^2\gamma_1^2}{\hbar^2 v^2}\right)\left(\frac{L^2\Delta^2}{\hbar^2 v^2}\right)\ln^2\left(\frac{4\gamma_1}{|\Delta|}\right). \quad (11)$$

The change of the total single-particle energy may be estimated by integrating the valence bands energies, $\epsilon_-^{(1)}$ and $\epsilon_-^{(2)}$, with respect to momentum over the circularly symmetrical Fermi surface:

$$E \approx \frac{2L^2}{\pi\hbar^2}\int p\,\mathrm{d}p\left[\epsilon_-^{(1)}(\Delta)+\epsilon_-^{(2)}(\Delta)-\epsilon_-^{(1)}(0)-\epsilon_-^{(2)}(0)\right].$$

On integrating from zero momentum to a large momentum p_∞, and expanding in Δ/γ_1, the change in the single particle energy for finite Δ, as compared to $\Delta = 0$, is

$$E \approx -\frac{\gamma_1}{8\pi}\left(\frac{L^2\Delta^2}{\hbar^2 v^2}\right)\left[\frac{1}{2}+\ln\left(\frac{4\gamma_1}{|\Delta|}\right)\right]. \quad (12)$$

The logarithmic dependence of the density equation (10) appears as the square of the infrared logarithm in the charging energy equation (11). Since the single particle energy equation (12) contains only a single infrared logarithm, the large energetic cost of charging an undoped bilayer ensures stability with respect to the opening of a gap in the absence of an applied external electric field.

The gap Δ between the conduction and valence bands arises from layer asymmetry so that, in contrast to monolayer graphene, there is a possibility of tuning the magnitude of the gap using external gates. Indeed, a gate is routinely used in experiments to control the density of electrons n on the bilayer system [1,2,8] and, in general, this will produce a simultaneous change in Δ. In the following we use a self-consistent Hartree approximation to determine the electronic distribution on the bilayer and the resulting band structure in the presence of an external gate.

As shown in Fig. 5, we consider the graphene bilayer, with interlayer separation c_0, to be located a distance d from a parallel metallic gate. The application of an external gate voltage $V_g = \mathrm{end}/\varepsilon_r'\varepsilon_0$ induces a total excess electronic density $n = n_1 + n_2$ on the bilayer system where n_1 (n_2) is the excess density on the layer closest to (furthest from) the gate (we use SI units). Here ε_0 is the permittivity of free space, ε_r' is the dielectric constant of the material between the gate and the bilayer, and e is the electronic charge. We assume that the screening of the effective charge density $\rho_+ = en$ from the metallic gate is not perfect, leading to an excess electronic density n_2 on the layer furthest from the gate. Considering a Gaussian surface, such as that shown with the dashed lines in Fig. 5, shows that the excess density n_2 gives rise to an electric field with magnitude $E = en_2/\varepsilon_r\varepsilon_0$ between the layers where ε_r is the nominal dielectric constant of the bilayer. There is a corresponding change in potential energy $\Delta U = e^2 n_2 c_0/\varepsilon_r\varepsilon_0$ that determines the layer asymmetry [16]:

$$\Delta(n) = \epsilon_2 - \epsilon_1 \equiv \frac{e^2 n_2 c_0}{\varepsilon_r\varepsilon_0}. \quad (13)$$

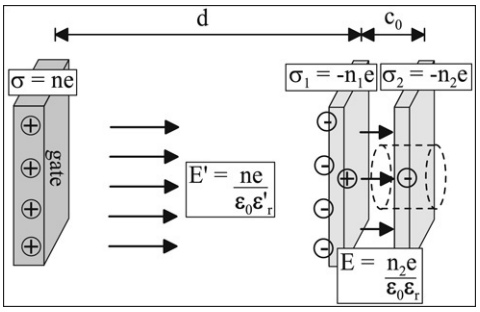

Fig. 5. Schematic of the graphene bilayer, with interlayer separation c_0, located a distance d from a parallel metallic gate. The gate voltage V_g induces a total excess electronic density $n = n_1 + n_2$ on the bilayer system where n_1 (n_2) is the excess density on the layer closest to (furthest from) the gate. The dashed line shows a Gaussian surface, from which it can be deduced that the magnitude of the electric field between the layers of the bilayer is $E = en_2/\varepsilon_r\varepsilon_0$.

In terms of the capacitance of a bilayer of area L^2, $C_b = \varepsilon_r\varepsilon_0 L^2/c_0$, this may be written $\Delta(n) = e^2 n_2 L^2/C_b$.

We self consistently calculate the excess densities n_1, n_2, $n = n_1 + n_2$, Eq. (9), and the gap Δ, Eq. (13). This has been done numerically in Ref. [16]. Analytically, for moderately low density, $4\pi\hbar^2 v^2|n| < \gamma_1^2$, we find

$$\Delta \approx \frac{e^2 L^2 n}{2C_b} f_\Lambda\left(\frac{\hbar^2 v^2 \pi |n|}{\gamma_1^2}\right), \quad (14)$$

$$f_\Lambda(x) \approx \frac{1}{1+\Lambda\left(x - \frac{1}{2}\ln x\right)}.$$

The function $f_\Lambda(x)$ is plotted in Fig. 4(b) for different values of the dimensionless parameter $\Lambda = e^2 L^2 \gamma_1/(2\pi\hbar^2 v^2 C_b)$ which describes the effectiveness of the interlayer screening of the bilayer. The limit $\Lambda \to 0$ describes poor screening when the density on each layer is equal to $n/2$ whereas for $\Lambda \to \infty$ there is excellent screening, the density lies solely on the layer closest to the external gate and $\Delta = 0$. Note that $f_\Lambda(x) \to 0$ as $x \to 0$ because of the logarithm, meaning that the effectiveness of interlayer screening increases upon lowering density. Using typical experimental parameters [22] we find $\Lambda \approx 1.3$. We estimate that the addition of density $n \sim 10^{12}$ cm^{-2} yields a gap $\Delta \sim 10$ meV [31].

6. Conclusions

We reviewed the results of tight-binding model studies of bilayer graphene and its low-energy electronic band structure. The optical absorption coefficient of a bilayer displays features related to the band structure on the energy scale of the order of the interlayer coupling $\gamma_1 \approx 0.4$ eV [18,19], in contrast to the featureless absorption coefficient of monolayer graphene. At much lower energies, $\epsilon_L \sim 1$ meV, trigonal warping of the band structure might produce a Lifshitz transition in which the isoenergetic line about each valley is broken into four pockets.

Inter-layer asymmetry creates a gap between the conduction and valence bands: bilayer graphene is a semiconductor with a tuneable gap of up to about 0.4 eV. However, by comparing the charging energy with the single particle energy, it is

possible to show that an undoped, gapless bilayer is stable with respect to the spontaneous opening of a gap via a ferroelectric transition. A self-consistent Hartree approximation was used to determine the density distribution of the two layers when the density n is varied using an asymmetrically placed gate, resulting in a density dependent gap $\Delta(n)$. Control of the gap has been modelled using the tight-binding model [16,17,12] and such calculations appear to be in good agreement with ARPES measurements [9], observations made in the regime of the quantum Hall effect [17], and density functional theory calculations [12].

The use of a single gate modulates the density and the gap simultaneously, but it should be possible to independently control the density and the gap by employing both a top and a bottom gate. This suggests a route to new nanoelectronic devices defined within a single sheet of gated bilayer graphene. In particular, one can use a combination of top and bottom gates to control the asymmetry gap in the bilayer spectrum and to define an array of quantum dots on a sizeable bilayer sheet. By localizing electrons on such dots and electrically controlling their coupling, this may enable one to produce arrays [32] of electron spin qubits for quantum information processing [33].

Acknowledgements

The authors thank I. Aleiner, A. K. Geim, K. Kechedzhi, P. Kim, K. Novoselov and L. M. K. Vandersypen for useful discussions and EPSRC for financial support.

References

[1] K.S. Novoselov, A.K. Geim, S.V. Morozov, D. Jiang, Y. Zhang, S.V. Dubonos, I.V. Grigorieva, A.A. Firsov, Science 306 (2004) 666.
[2] K.S. Novoselov, A.K. Geim, S.V. Morozov, D. Jiang, M.I. Katsnelson, I.V. Grigorieva, S.V. Dubonos, A.A. Firsov, Nature 438 (2005) 197;
Y.B. Zhang, Y.W. Tan, H.L. Stormer, P. Kim, Nature 438 (2005) 201.
[3] D. DiVincenzo, E. Mele, Phys. Rev. B 29 (1984) 1685.
[4] G.W. Semenoff, Phys. Rev. Lett. 53 (1984) 2449.
[5] F.D.M. Haldane, Phys. Rev. Lett. 61 (1988) 2015;
Y. Zheng, T. Ando, Phys. Rev. B 65 (2002) 245420;
N.M.R. Peres, F. Guinea, A.H. Castro Neto, Phys. Rev. B 73 (2006) 125411;
A.H. Castro Neto, F. Guinea, N.M.R. Peres, Phys. Rev. B 73 (2006) 205408.
[6] T. Ando, T. Nakanishi, R. Saito, J. Phys. Soc. Japan 67 (1998) 2857.
[7] E. McCann, V.I. Fal'ko, Phys. Rev. Lett. 96 (2006) 086805.
[8] K.S. Novoselov, E. McCann, S.V. Morozov, V.I. Fal'ko, M.I. Katsnelson, U. Zeitler, D. Jiang, F. Schedin, A.K. Geim, Nature Phys. 2 (2006) 177.
[9] T. Ohta, A. Bostwick, T. Seyller, K. Horn, E. Rotenberg, Science 313 (2006) 951.
[10] S.B. Trickey, F. Müller-Plathe, G.H.F. Diercksen, J.C. Boettger, Phys. Rev. B 45 (1992) 4460.
[11] S. Latil, L. Henrard, Phys. Rev. Lett. 97 (2006) 036803.
[12] H. Min, B.R. Sahu, S.K. Banerjee, A.H. MacDonald, Phys. Rev. B 75 (2007) 155115.
[13] K. Yoshizawa, T. Kato, T. Yamabe, J. Chem. Phys. 105 (1996) 2099;
T. Yumura, K. Yoshizawa, J. Chem. Phys. 279 (2002) 111.
[14] C.L. Lu, C.P. Chang, Y.C. Huang, R.B. Chen, M.L. Lin, Phys. Rev. B 73 (2006) 144427;
J. Nilsson, A.H. Castro Neto, N.M.R. Peres, F. Guinea, Phys. Rev. B 73 (2006) 214418;
M. Koshino, T. Ando, Phys. Rev. B 73 (2006) 245403;
F. Guinea, A.H. Castro Neto, N.M.R. Peres, Phys. Rev. B 73 (2006) 245426;
M.I. Katsnelson, Eur. Phys. J. B 51 (2006) 157; 52 (2006) 151.
[15] B. Partoens, F.M. Peeters, Phys. Rev. B 74 (2006) 075404.
[16] E. McCann, Phys. Rev. B 74 (2006) 161403.
[17] E.V. Castro, K.S. Novoselov, S.V. Morozov, N.M.R. Peres, J.M.B. Lopes dos Santos, J. Nilsson, F. Guinea, A.K. Geim, A.H. Castro Neto. cond-mat/0611342.
[18] J. Nilsson, A.H. Castro Neto, F. Guinea, N.M.R. Peres, Phys. Rev. Lett. 97 (2006) 266801.
[19] D.S.L. Abergel, V.I. Fal'ko, Phys. Rev. B 75 (2007) 155430.
[20] P.R. Wallace, Phys. Rev. 71 (1947) 622;
J.C. Slonczewski, P.R. Weiss, Phys. Rev. 109 (1958) 272.
[21] M.S. Dresselhaus, G. Dresselhaus, Adv. Phys. 51 (2002) 1;
R.C. Tatar, S. Rabii, Phys. Rev. B 25 (1982) 4126;
J.-C. Charlier, X. Gonze, J.-P. Michenaud, Phys. Rev. B 43 (1991) 4579.
[22] We use $\gamma_1 = 0.39$ eV [21,9], $v_3/v = 0.1$, $v = 8.0 \times 10^5$ m/s [2], $c_0 = 3.35$ Å, and $\varepsilon_r = 1$.
[23] Corners of the hexagonal Brillioin zone are $\mathbf{K}_\xi = \xi(\frac{4}{3}\pi a^{-1}, 0)$, where $\xi = \pm 1$ and a is the lattice constant.
[24] V. Gusynin, S. Sharapov, J. Carbotte, Phys. Rev. Lett. 96 (2006) 256802;
V. Gusynin, S. Sharapov, Phys. Rev. B 73 (2006) 245411.
[25] L. Falkovsky, A. Varlamov. cond-mat/0606800.
[26] J. Cserti, Phys. Rev. B 75 (2007) 033405.
[27] For $\hbar\omega \ll \frac{1}{4}\gamma_1$ this result transforms into $f_2 = 1$ suggested by Cserti [26] for the microwave absorption in bilayer graphene. However one should be aware that Eq. (5) and conclusions of Ref. [26] cannot be applied to $\hbar\omega < \epsilon_L = \frac{1}{4}\gamma_1(v_3/v)^2 \sim 1$ meV. At $\epsilon_F \approx \epsilon_L$, trigonal warping term causes the Lifshitz transition in the topology of the Fermi line in each valley as explained in Section 4.
[28] G. Dresselhaus, Phys. Rev. B 10 (1974) 3602;
K. Nakao, J. Phys. Soc. Japan 40 (1976) 761;
M. Inoue, J. Phys. Soc. Japan 17 (1962) 808;
O.P. Gupta, P.R. Wallace, Phys. Status. Solidi. B 54 (1972) 53.
[29] At energies below the Lifshitz transition [7], the bilayer spectrum in each of the four Fermi surface pockets is linear, and the integral Berry phase 2π in bilayer graphene [7,8] is divided into Berry phase π in each of the three side pockets and $-\pi$ in the central one.
[30] Note that the "mexican hat" structure of the low energy bands means that the true value of the gap $\tilde{\Delta} = |\Delta|\gamma_1/\sqrt{\gamma_1^2 + \Delta^2}$ occurs at finite momentum $p_g = |\Delta|/(2v)\sqrt{(2\gamma_1^2 + \Delta^2)/(\gamma_1^2 + \Delta^2)}$ away from the K point. For huge values of the asymmetry $|\Delta| \gg \gamma_1$, the gap would saturate at $\tilde{\Delta} \approx \gamma_1$ although for modest asymmetry values $|\Delta| \ll \gamma_1$, the relation is simply $\tilde{\Delta} \approx |\Delta|$.
[31] In Section 5 we neglected the role of additional weak couplings, such as $A1$–$B2$ coupling γ_3 that results in trigonal warping, Section 4, and is relevant at low density $n \sim 1 \times 10^{11}$ cm^{-2}. Indeed, trigonal warping should result in a small overlap between the conduction and valence band of ≈2 meV.
[32] V.I. Fal'ko, Nature Phys. 3 (2007) 151.
[33] D. Loss, D.P. DiVincenzo, Phys. Rev. A 57 (1998) 120.